BIOCHEMISTRY
including biophysical chemistry & molecular biology

Article

pubs.acs.org/biochemistry

Dual Allosteric Inhibitors Jointly Modulate Protein Structure and Dynamics in the Hepatitis C Virus Polymerase

Jodian A. Brown and Ian F. Thorpe*

Department of Chemistry and Biochemistry, University of Maryland Baltimore County, Baltimore, Maryland 21250, United States

Supporting Information

ABSTRACT: The hepatitis C virus (HCV) infects close to 200 million people globally, resulting in a significant need for effective HCV therapies. The HCV polymerase (gene product NS5B) is a valuable target for therapeutics because of its role in replicating the viral genome. Various studies have identified inhibitors for this enzyme, including non-nucleoside inhibitors (NNIs) that bind distal to the enzyme active site. Recently, it has been shown that simultaneously challenging the enzyme with two NNIs results in enhanced inhibition relative to that observed after challenge with individual inhibitors, suggesting that employing multiple NNIs might be the basis of more effective therapeutics. Nevertheless, the molecular mechanisms responsible for this enhanced inhibition remain unclear. We employ molecular dynamics simulations to determine the origin of enhanced inhibition when two NNIs bind to NS5B. Our results suggest that nonoverlapping NNI sites are compatible with simultaneous binding of dual NNIs. We observe that both inhibitors act in concert to induce novel enzyme conformations and dynamics, allowing us to identify molecular mechanisms underlying enhanced inhibition of NS5B. This knowledge will be useful in optimizing combinations of NNIs to target NS5B, helping to prevent the acquisition of viral resistance that remains a significant barrier to the development of HCV therapeutics.

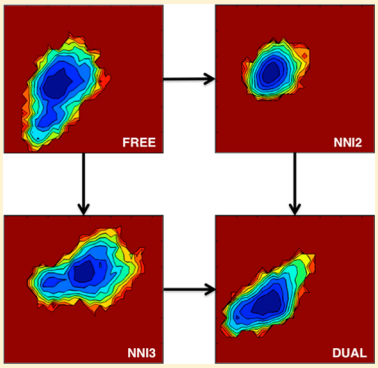

The hepatitis C virus (HCV) is a global health challenge, affecting approximately 200 million people worldwide, of which 4 million are Americans.[1,2] In the United States, this viral infection results in cirrhosis of the liver and is the principal cause of liver transplantation.[1] There are six distinct genotypes of HCV with various subtypes. Of particular interest is genotype 1 (subtypes a and b), the most prevalent strain in North America. Infections by this genotype are particularly difficult to treat, with the current U.S. Food and Drug Administration-approved standard of care for HCV (ribavirin and interferon α) being markedly less effective against this genotype.[3] Unfortunately, current therapies are ineffective in treating up to half of all HCV-affected patients, especially those infected with genotype 1.[3,4] Recently, Gilead Sciences introduced Sovaldi, a new direct acting antiviral agent targeting the HCV polymerase that exhibits weakened side effects and decreased treatment times. However, this drug is most effective when used in combination with ribavirin and interferon α and is also very expensive. Treatment regimens involving ribavirin and interferon α are not ideal, as these therapeutics are known to induce adverse side effects. Consequently, there is still a need for new and less expensive polymerase inhibitors that could serve as therapeutics, as well as to understand the mechanisms of action of such molecules.

The HCV genome encodes several structural and non-structural proteins. The nonstructural protein NS5B is an RNA-dependent RNA polymerase critical for viral replication[5] and is at the center of many biochemical and drug design studies. NS5B has three canonical polymerase domains (the palm, thumb, and fingers regions) that encircle the active site (Figure 1).[6,7] Thus far, crystallographic data show at least four distinct allosteric sites on NS5B to which non-nucleoside inhibitors (NNIs) bind, with two sites each in the palm and thumb domains (Figure 1).[1,8] Thumb sites I and II (known as NNI1 and NNI2, respectively) are located at the top and base of the thumb domain, respectively (see Figure 1). The palm sites partially overlap and are differentiated on the basis of palm site I (NNI3) being located closer to the interface between the palm and thumb domains, while palm site II (NNI4) extends into the arginine 200 hinge region that is closer to the active site.[1,8] NNIs span a range of chemical scaffolds that can bind to different regions within the known binding sites. However, most fail after entering into clinical trials because of the development of unforeseen toxicities.[1,9] Many studies have identified and optimized inhibitors specific to the active site as well as allosteric pockets of NS5B. Active site inhibitors have been more successful in the clinic but have a higher risk of targeting host polymerases compared to allosteric inhibitors, the latter being more specific to viral polymerases.[1,10,11] Thus, by targeting the allosteric pockets of NS5B, one may reduce the number of nonspecific interactions that are problematic for active site inhibitors. Furthermore, NS5B possesses multiple allosteric sites, which provides for the possibility of using several NNIs in combination.

Received: April 16, 2015
Revised: June 3, 2015
Published: June 11, 2015

DOI: 10.1021/acs.biochem.5b00411
Biochemistry 2015, 54, 4131−4141

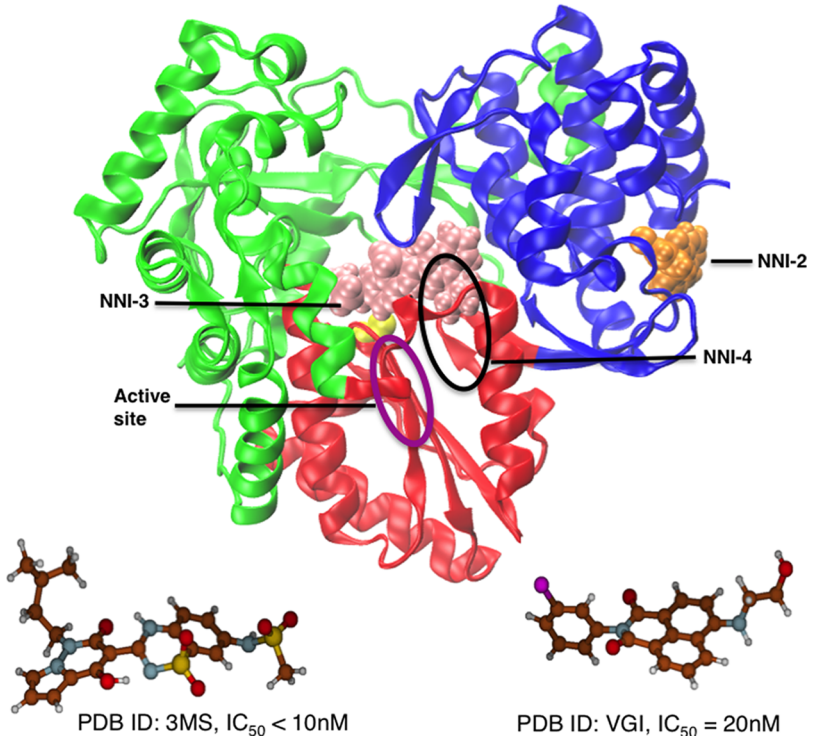

Figure 1. Structure of the hepatitis C virus polymerase (NS5B) depicting three allosteric binding sites. The three domains are colored red (palm), blue (thumb), and green (fingers). The two magnesium ions needed for efficient viral replication are depicted as yellow van der Waals spheres and the active site encircled by the magenta oval. The two allosteric inhibitors employed in this work are shown as van der Waals spheres in their respective binding sites (VGI colored orange and 3MS pink).

Despite these positive features of NNIs, there are several challenges impeding the use of such inhibitors in the clinic. One such challenge is the fact that genetic mutations can arise in NS5B that allow it to become resistant to NNIs. This problem is exacerbated by the lack of proofreading activity in NS5B during replication, which results in low fidelity and an increased risk for mutations that makes it more likely for resistance to emerge.[1,5,9] Consequently, there is an urgent need to circumvent HCV resistance to NS5B inhibitors such as NNIs.

It is possible that viral resistance to NNIs can be overcome by employing multiple NNIs in concert. The simultaneous application of NNIs targeting nonoverlapping binding sites has been shown to enhance inhibition of NS5B. For instance, studies involving the use of both benzothiazine (NNI3) and benzimidazole (NNI1) inhibitors have demonstrated enhanced inhibition relative to application of either compound individually (see Figure 1 for site locations).[11,12] There have also been studies combining pyridine carboxamide (NNI4) and dihydropyranone (NNI2) inhibitors, resulting in enhanced inhibition.[13] However, the molecular mechanisms that govern allosteric inhibition are still largely unknown, particularly when multiple allosteric inhibitors are applied in combination. In this work, we employ molecular simulations and binding free energy calculations to understand the molecular mechanisms that govern enhanced inhibitory effects when allosteric ligands simultaneously bind to the NNI2 and NNI3 sites on the enzyme. Our results suggest that simultaneous binding of inhibitors at both sites is possible and that the presence of dual inhibitors induces synergistic changes to enzyme conformation and dynamics.

MATERIALS AND METHODS

Biomolecular Systems. A crystal structure of NS5B from HCV genotype 1b [Protein Data Bank (PDB) entry 1QUV] was used in our simulations. 1QUV was selected because it has a relatively high resolution of 2.5 Å and does not contain any ligand. This allows us to clearly observe the impact of ligand binding on enzyme structure and dynamics. 1QUV consists of a single amino acid chain containing 578 residues. However, the last 47 C-terminal residues were removed because they are not essential for *in vitro* RNA replication.[14,15] These residues may play a role in docking the virus to the endoplasmic reticulum of the host *in vivo*.[14,16] Prior work from our group has shown that these residues reduce the conformational sampling and overall flexibility of the enzyme. They also induce a conformation that may disfavor *de novo* initiation *in vitro*.[17] The three-dimensional structure of 1QUV was determined without metal ions coordinated within the active site. However, two magnesium ions were added to the structure in all simulations because they have been shown biochemically to be needed for efficient enzyme function[18,19] and have been observed to fundamentally alter the structure and dynamics of the enzyme in previous molecular simulations by our group.[15] Two allosteric inhibitors, 3MS and VGI, were employed in this work. Both inhibitors have been separately cocrystallized with NS5B of genotype 1b and show nanomolar activities against the enzyme individually [for 3MS, IC_{50} < 10 nM (from PDB entry 3CO9); for VGI, IC_{50} = 20 nM (from PDB entry 2WHO)].[20,21] These ligands were chosen because they bind to nonoverlapping allosteric sites that have been implicated in enhanced inhibition of NS5B when used in combination.[12,13,22] In addition, the ligands individually have been used in previous simulations, providing a way to independently assess the robustness of our current

DOI: 10.1021/acs.biochem.5b00411
Biochemistry 2015, 54, 4131−4141

findings.[15,17] To understand the impact of each inhibitor on the enzyme, we performed simulations in which only one of each ligand was bound (these will be termed NNI3 and NNI2 for 3MS and VGI, respectively, throughout), while our control system was that of the free protein (FREE). Our fourth system consisted of 1QUV bound to both ligands (DUAL). In each simulation, 19 chloride ions were added to neutralize the total system charge. Each system was solvated with explicit TIP3P water molecules within a truncated octahedral unit cell larger than the protein by 10 Å in each dimension, resulting in an edge length of at least 91 Å (Table 1).

Table 1. Each System with Its Corresponding Identifier, Total Simulation Length, Cell Length, Total Number of Water Atoms, and Total Number of Atoms in Each Simulation

system components (identifier)	total simulation time (ns)	truncated octahedron unit cell length (Å)	total no. of water residues	total no. of atoms
1QUV (FREE)	1000	91.5244	17360	60391
1QUV and VGI (NNI2)	1000	91.6288	17343	60381
1QUV and 3MS (NNI3)	1000	91.5259	17353	60426
1QUV, 3MS, and VGI (DUAL)	1002	91.5746	17331	60401
3MS	10	35.3453	1101	3359
VGI	10	34.4103	1030	3131

Minimization and Molecular Dynamics Simulations. The force field parameters for VGI and 3MS were taken from CHARMM general force field versions 2b6 and 2b7, respectively. Parameters not available in the ligand force field were obtained using the procedure described by MacKerell and co-workers.[23,24] The CHARMM27 protein force field was used to describe the protein.[25] Before simulations were begun, the solvated free enzyme and ligand-bound systems were minimized with NAMD version 2.7 using the steepest descent method for a total of 1000 steps. After minimization, all MD simulations were conducted at a temperature of 300 K. Initially, the protein backbone for each system was restrained using a force constant of 10 kcal mol^{-1} Å^{-2} applied to α-carbons during 5 ns of initial *NVT* simulation. This was followed by 5 ns simulations in the *NPT* ensemble employing the Berendsen barostat, maintaining a pressure of 1.01 bar and without any restraints on the protein backbone. Finally, production runs were conducted in the *NVT* ensemble. At each stage, the temperature was maintained via velocity reassignment for at least every 1000 steps for FREE, NNI2, and NNI3. For DUAL, a Langevin thermostat with friction coefficients of 10 and 1 ps^{-1} was applied to non-hydrogen atoms for the *NPT* and *NVT* runs, respectively (a value of 5 ps^{-1} was employed for the first 80 ns of the *NVT* run). Different thermostats were used to achieve optimal computational efficiency, and their use was not observed to alter the simulation properties. For all systems, we conducted production simulations for a total of at least 1 μs in 10 ns increments with an integration time step of 2 fs. During the production simulations, trajectory coordinates were written out at least every 100 ps. For all analyses, we utilized the last 500 ns of each trajectory.

We also performed MD simulations containing only the ligands to compute the ligand entropy contribution to relative binding free energies. We utilized the same minimization protocol for the solvated systems of VGI and 3MS (see Table 1 for solvated systems) followed by MD for 5 ns in the *NPT* ensemble using the Berendsen barostat to maintain an average pressure of 1.01 bar and the Langevin thermostat with a friction coefficient of 1 ps^{-1} applied to non-hydrogen atoms. The Langevin thermostat was also employed to perform 10 ns *NVT* production runs for each solvated ligand system.

Covariance. One mechanism by which allosteric inhibitors may work is by disrupting motions that are critical to protein function. Consequently, we performed covariance analysis as shown in eq 1 to understand the characteristic motions of protein atoms within the trajectories. The covariance $C_{i,j}$ between sites i and j is defined by

$$C_{i,j} = \frac{\langle (r_i - \langle r_i \rangle)(r_j - \langle r_j \rangle) \rangle}{\sqrt{\langle (r_i - \langle r_i \rangle)^2 \langle (r_j - \langle r_j \rangle)^2}} \quad (1)$$

In eq 1, r_i represents the position of the center of mass for residue i and the angle brackets denote ensemble averages.

Principal Component Analysis. To reduce the dimension of our data and more readily identify the principal motions in each system, we performed principal component analyses (PCA) of the covariance matrix.

$$[\mathbf{V}][C_{i,j}][\mathbf{V}^{\mathbf{T}}] = \mathrm{diag}[\lambda_1, \lambda_2, \lambda_3, \ldots] \quad (2)$$

The covariance matrix ($C_{i,j}$) was diagonalized using the eigenvector matrix ($\mathbf{V}$) to generate eigenvalues (λ). The eigenvectors and eigenvalues comprise the principal components of the NS5B motions. PCA aids in characterizing changes in atomic motions by allowing us to examine the primary vibrational modes within each biomolecular system.

Root-Mean-Square Fluctuations (rmsf's). The rmsf provides a measure of local flexibility in the protein. We calculated the rmsf for each residue center of mass by aligning every snapshot to the initial crystal structure and summing the difference between the instantaneous position of each center of mass at time t_j, ($r_i(t_j)$), and its corresponding reference position ($\tilde{r}_i$) for every snapshot.

$$\mathrm{rmsf}_i = \sqrt{\frac{\sum_{t_j}^{T} [r_i(t_j) - \tilde{r}_i]^2}{N}} \quad (3)$$

This difference is then divided by the total number of snapshots (N) and the square root taken of this result.

Describing the Enzyme Conformational Space. Previous studies indicate that at least two protein conformations are necessary for viral replication.[26,27] A closed conformation is thought to be essential for the initiation stage of replication, while an open conformation is important for the elongation phase. To monitor the different protein conformations adopted throughout the simulations, we used two structural metrics. (i) The interdomain angle is the angle among the fingers, palm, and thumb subdomains and allows us to determine how open or closed the enzyme is during a given trajectory. The interdomain angle was computed via measuring the angle between the centers of mass for each protein subdomain. (ii) The template channel is critical for the binding of the RNA template. Consequently, we measured the widths of the channel to understand the impact of inhibitor binding on this crucial structural element. To probe the template channel width, the distance between the centers of mass of residues

DOI: 10.1021/acs.biochem.5b00411
Biochemistry 2015, 54, 4131−4141

methionine 139 and valine 405 was calculated. More open states of the enzyme are associated with larger values of these two metrics.

Hydrogen Bonding. We employed the hydrogen bond (Hbond) utility in CHARMM to calculate Hbond distances and lifetimes of each system. We used the default hydrogen−acceptor probe distance of 2.4 Å and counted hydrogen bonds as interactions with occupancies of at least 10% for protein−ligand interactions and 20−90% for protein−protein interactions.

Binding Free Energies. To assess relative binding free energies, we used the Molecular Mechanics-Generalized Born Surface Area (MM-GBSA) free energy method. We employed the CHARMM Generalized Born Molecular Volume module (analytical method II) for these calculations using a surface area coefficient of 0.00542 kcal mol^{-1} Å^{-2}.[28−31] The ligand binding free energy ΔG was computed according to the equation $\Delta G = \Delta H - T\Delta S$ for the singly and doubly bound ligand simulations as follows:

For the singly bound system

$$\mathrm{NS5B(aq)} + \mathrm{L(g)} \xrightarrow{\Delta G_x} \mathrm{NS5B{\cdot}L(aq)} \quad (4)$$

For the doubly bound system

$$\mathrm{NS5B(aq)} + \mathrm{L1(g)} + \mathrm{L2(g)} \xrightarrow{\Delta G_x} \mathrm{NS5B{\cdot}L1{\cdot}L2(aq)} \quad (5)$$

In eqs 4 and 5, L denotes either the NNI2 or NNI3 ligand that is present in the protein−ligand complex on the right-hand side while x corresponds to ΔG with respect to NNI2, NNI3, or DUAL. ΔH values were calculated using eq 6. ΔS was calculated using eq 7 and employed the quasi-harmonic approximation as implemented in the CHARMM VIBRAN module to evaluate the protein or ligand entropy. In each case, only the 1% of modes with the lowest frequencies were employed for the entropy calculations. This choice was made because the lowest-frequency modes typically account for most of the overall fluctuation in molecular systems. Thus, focusing on these modes generates a more representative description of the entropy changes mediated by large amplitude fluctuations. It is these fluctuations (rather than small amplitude, high-frequency vibrations) that are most likely to be functionally relevant in biomolecular systems. The calculation was performed using trajectories of the centers of mass of enzyme residues for the protein entropy or using ligand all-atom trajectories for the ligand entropy. For eq 7, $S_{\text{free protein}}$ and $S_{\text{free ligand}}$ refer to the entropies computed from the simulations of only the protein and only the ligand, respectively. Note that this treatment neglects the changes in rotational and translational ligand entropy and captures the solvation entropy only qualitatively via the impact of the Generalized Born solvation term on ΔH. Nonetheless, we anticipate that these quantities are consistent for either ligand, allowing the trends in binding affinity to be reproduced well upon comparison of the binding of individual ligands for NNI2 and NNI3 to that of DUAL.

$$\Delta H = H_{\text{complex}} - H_{\text{protein from complex}} - H_{\text{ligand from complex}} \quad (6)$$

$$\Delta S = (S_{\text{protein from complex}} - S_{\text{free protein}}) + (S_{\text{ligand from complex}} - S_{\text{free ligand}}) \quad (7)$$

In this context, one would anticipate that synergistic binding in DUAL would be reflected in a more favorable binding free energy for the DUAL system than for the sum of the individual binding free energies for NNI2 and NNI3. Thus, synergy in binding would be consistent with the inequality $\Delta G_{\text{DUAL}} < \Delta G_{\text{NNI2}} + \Delta G_{\text{NNI3}}$.

RESULTS AND DISCUSSION

NNI2 and NNI3 Display Distinct Impacts on NS5B Conformations and Dynamics. To understand the impact of ligand binding on conformational sampling, we calculated two-dimensional potentials of mean force (PMFs) using both the interdomain angle and the template channel width as coordinates (Figure 2 and Table 2). In the PMF of the FREE enzyme, we observe a minimum centered at an interdomain angle of ∼67° while fluctuations of the template channel width are between 10.3 and 20.2 Å (Figure 2A). In

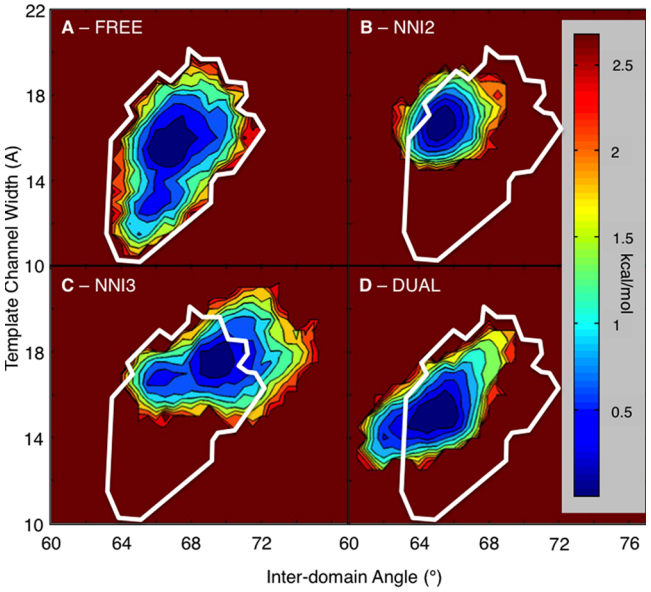

Figure 2. Dual inhibitor binding results in novel NS5B conformations. Two-dimensional potential of mean force plots of template channel width vs interdomain angle for the (A) FREE, (B) NNI2, (C) NNI3, and (D) DUAL systems. The color bar represents the relative free energies in units of kilocalories per mole, where blue indicates more favorable energies and red less favorable energies. The white line demarcates the conformational space sampled in the FREE system to highlight differences between the FREE and ligand-bound simulations.

Table 2. Interdomain Angles and Template Channel Widths for PDB Structures Discussed in the Text and Average Structures from Each of the Four Simulations

system	interdomain angle (deg)	template channel width (Å)
1QUV	70.045	16.77
1NB7 (RNA template present)	68.57	16.53
1YUY	70.33	16.59
1YV2	71.47	18.6
FREE[a]	67.04	15.37
NNI2[a]	65.42	16.72
NNI3[a]	69.48	17.48
DUAL[a]	64.79	15.21

[a]Mean values over the last 500 ns of MD simulations for each respective system.

DOI: 10.1021/acs.biochem.5b00411
Biochemistry 2015, 54, 4131−4141

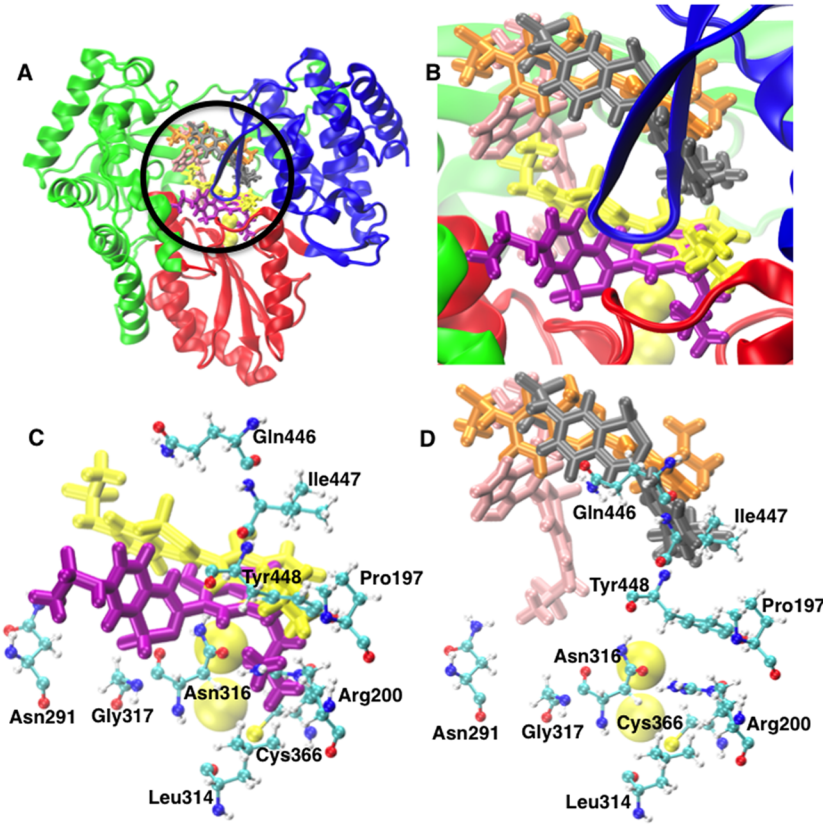

Figure 3. Conformations and locations of 3MS in the NNI3 and DUAL systems suggest a single expansive palm-binding cavity. Panel A depicts snapshots of both the NNI3 and DUAL systems relative to the three protein domains, while panel B is a close-up image of the black encircled region in panel A. Panels C and D show snapshots of 3MS (licorice representation) from NNI3 and DUAL simulations, respectively, along with critical protein residues (CPK representation) known to bind different palm allosteric moieties. These residues represent key interactions for specific palm allosteric inhibitors. In panel D, 3MS is shown interacting with palm residues known to be involved in binding to other palm inhibitors. In panel C, the yellow- and purple-colored snapshots of 3MS are taken from the NNI3 trajectory and represent different orientations that facilitate protein−ligand interactions specific to the two known palm allosteric sites. In panels B and D, the pink, orange, and black snapshots of 3MS highlight different orientations of the ligand within the DUAL trajectory and how these allow for varying protein−ligand interactions.

contrast, the NNI2 system displays a more compact minimum centered at an angle of ∼65.5° and displays a narrower range of template channel widths of 14.6−19.8 Å (Figure 2B). Thus, in comparison to FREE, the presence of the NNI2 ligand restricts conformational sampling of the enzyme. Similar observations were noted in other recent work from our group.[17] We believe that the ability of the NNI2 ligand to predominantly stabilize more closed conformations likely prevents the transitions between closed and open conformations that NS5B must undergo to perform its function, hindering replication. In contrast to NNI2, NNI3 has a minimum that is less compact (Figure 2C). The enzyme samples interdomain angles and template channel widths larger than those of FREE and thus explores conformational states that are in general more open. Thus, both allosteric inhibitors are similar in that they restrict conformational sampling, although this restriction is directed toward different regions of the free energy landscape.

It is important to note that a majority of the NNI3 population displays quite large interdomain angle values, some of which are not observed in the FREE enzyme. This suggests that the NNI3 ligand (3MS) is able to induce novel conformations not observed for the FREE enzyme. We believe one reason for this observation is the extensive fluctuations of 3MS (Figure 3C) and its ability to interact with all three protein domains. The primarily horizontal conformation of 3MS within the central cavity of the enzyme in NNI3 makes it difficult for interactions between thumb and fingers domains to stabilize closed conformations as observed in NNI2 or FREE. As the closed conformation is required for the initiation of RNA synthesis, the ability of 3MS to induce the enzyme to sample more open states would likely impede this stage of replication.

In NNI2, we see reduced correlated motions compared to those in the FREE system (e.g., see the decreased negative correlations in areas i, ii, and iv of Figure 4A). Area i of NNI2 shown in Figure 4A represents part of the thumb domain that includes key residues with which the ligand interacts directly such as Ser476, Tyr477, Met423, and Ile482. This area of eliminated motions also includes functional region III (residues 401−414) that is thought to play a role in nascent RNA duplex binding.[32] Flexibility in this area may be required to accommodate double-stranded RNA. Thus, eliminating these motions may weaken the ability of NS5B to bind the RNA duplex. Comparing the rmsf computed using the centers of mass of the protein residues for FREE and NNI2 shows that the flexibility of residues in functional region III is reduced because of the presence of the NNI2 ligand (Figure 5A). In addition to residues within the NNI2-binding pocket, we observed perturbed correlated movements within areas ii and iv of Figure 4A that span all three enzyme domains. Areas ii and iv constitute motifs B (residues 287−306) and E (residues 354−372) that function in template and nascent RNA 3′-end

DOI: 10.1021/acs.biochem.5b00411
Biochemistry 2015, 54, 4131−4141

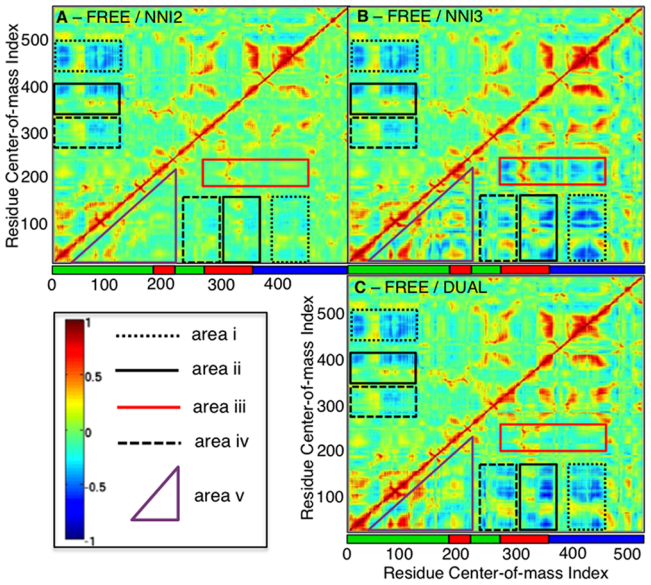

Figure 4. Correlation maps showing the impact of inhibitor binding on enzyme dynamics. In each map, the diagonal separates the FREE from the ligand-bound system, with the FREE being above the diagonal: (A) FREE vs NNI2, (B) FREE vs NNI3, and (C) FREE vs DUAL. The outlined areas consist of residues that constitute the ligand-binding sites or functional motifs that experience changes in protein motions.

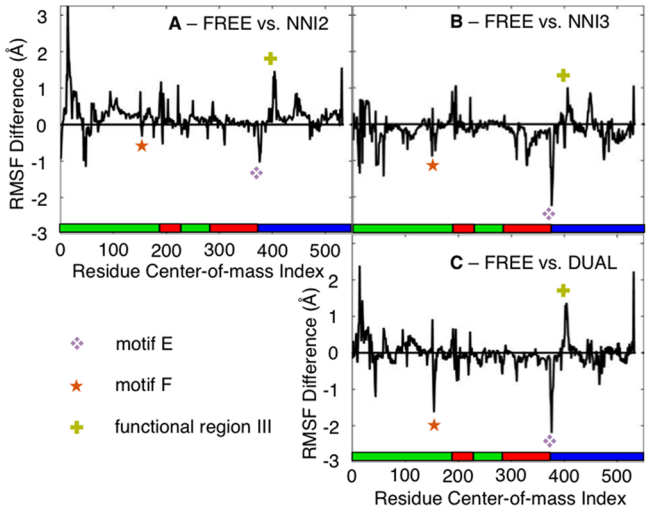

Figure 5. rmsf plots showing changes to the local enzyme flexibility in the presence of allosteric inhibitors. Each plot represents the difference between free and inhibitor-bound fluctuations. Values greater than zero indicate increased flexibility in the FREE compared to the ligand-bound system of interest, while values of less than zero denote increased flexibility for the respective ligand-bound system (A) NNI2, (B) NNI3, or (C) DUAL. The horizontal color bar demarcates the three enzyme domains: palm (red), thumb (blue), and fingers (green). The position of important functional and structural motifs is indicated as shown in the legend at the bottom left.

binding, respectively.[32] Thus, the NNI2 ligand is able to disrupt correlated motions not only with residues with which it directly interacts but also with residues that are located distal to its binding site. If the correlated motions observed within these key motifs are necessary for interactions between the enzyme and the indicated components of the replication complex to occur, the observed disruption could contribute to inhibiting NS5B function and thus reducing the extent of viral replication.

In contrast to NNI2, new correlations are induced in NNI3 when compared to those in FREE (e.g., the negative correlations in areas iii and v of NNI3 in Figure 4B). In addition, there are changes in the intensities and patterns of negative correlation in areas i, ii, and iv. In the crystal structure containing the NNI3 inhibitor bound to NS5B (PDB entry 3CO9), the inhibitor forms hydrogen bonds to Ser288, Tyr448, and Gln449 and interacts with other residues such as Phe193, Arg200, and Leu384 located within regions iii and v of Figure 4B. These interactions are recapitulated in our simulations. However, these regions of the enzyme also display new negative correlations compared to the FREE enzyme, suggesting that the NNI3 inhibitor induces new protein motions within its binding pocket. Changes in the patterns of correlated movement observed in areas i, ii, and iv (the latter two constituting motifs B and E, respectively) indicate that the NNI3 inhibitor can also modulate protein correlations distal to its binding pocket in a manner that would tend to reduce enzyme activity. rmsf data for NNI3 display an increase in the flexibility of residues in motifs E and F that exhibit new correlations (Figure 5B). As mentioned previously, motif E plays a role in binding the 3′-end of nascent RNA, while motif F plays a role in nucleotide and template binding. Unlike that of NNI2, the presence of the inhibitor in NNI3 seems to increase the number of fluctuations of residues within these motifs. Such fluctuations may work to destabilize these areas of the enzyme to the extent that they weaken interactions between NS5B and RNA template or nucleotides, thus inhibiting the enzyme. Thus, the NNI2 and NNI3 inhibitors may have contrasting effects in modulating the flexibility of these key regions yet may both ultimately reduce enzyme activity.

Dual Inhibitor Binding Induces Novel Protein Conformations and Dynamics. We find that even though VGI (NNI2) and 3MS (NNI3) have distinct impacts on certain structural features of the enzyme, they are able to bind simultaneously and jointly impact both structure and dynamics. To date, only biochemical data have been available to suggest that the combined presence of thumb inhibitors such as VGI and palm ligands like 3MS results in enhanced reductions of NS5B activity.[12,13,22] Thus, we provide the first molecular evidence that inhibitors at the thumb NNI2 and palm NNI3 sites are able to bind to the enzyme simultaneously and also delineate molecular mechanisms through which enhanced inhibition of NS5B via the action of dual allosteric inhibitors may occur. When both inhibitors are bound, we observe novel fluctuations in addition to patterns of protein motions that exhibit characteristics of the individual singly bound systems. There are patterns of correlation in areas i and ii of the correlation map for the DUAL system that also occur in the other systems, while there are patterns of correlation in area iv of the DUAL system that are more extensive and more intense compared to those in the other three systems (Figure 4C). The changes within area iv span two motifs: B, which has a functional role in primer and metal binding and catalysis as we mentioned previously, and C, which is important for triphosphate and nucleotide triphosphate binding and catalysis.[32] Novel fluctuations are also apparent in the significant increase in the flexibility of motif F in DUAL when compared to those in the NNI3 and FREE systems (Figure 5B,C). Motif F has functional roles in nucleotide and template binding.[32] Increased fluctuations in these motifs may

DOI: 10.1021/acs.biochem.5b00411
Biochemistry 2015, 54, 4131−4141

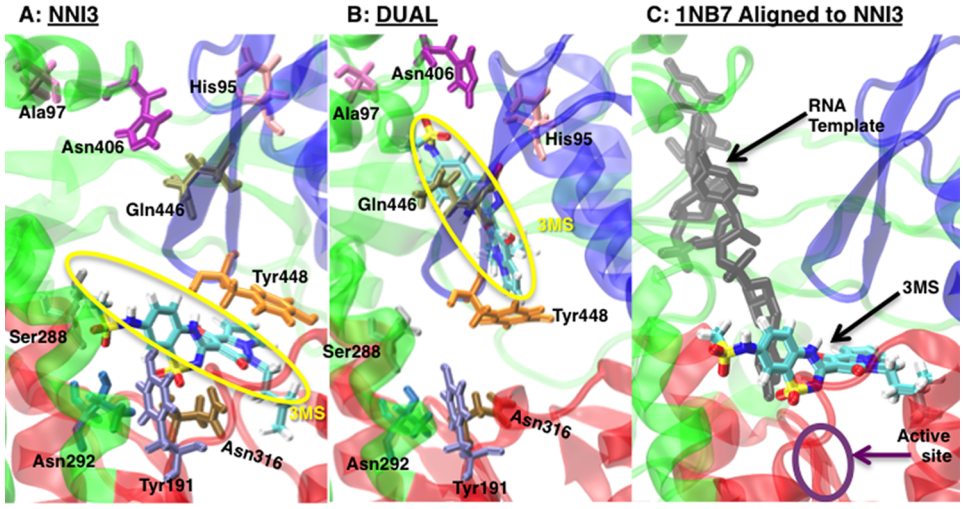

Figure 6. Comparison of key hydrogen bonds involving the 3MS ligand in the (A) NNI3 and (B) DUAL systems. We chose two snapshots that are both in a closed conformation (interdomain angle of <68°), which emphasizes the local differences around the inhibitor even though the global conformations are similar. For each panel, the protein is translucent to allow for better visibility of the important residues in the hydrogen bond network. (C) Alignment of NNI3 snapshot 4000 and PDB entry 1NB7, a structure of NS5B containing short RNA template, to show how the presence of 3MS prevents access of the template to the active site.

drastically reduce or prevent interactions between the enzyme and template and/or nucleotides. Thus, these new protein motions in the DUAL system may impair viral replication by disrupting catalysis at the active site. This finding may represent one mechanism by which enhanced inhibition of the viral enzyme is mediated in the presence of dual NNIs.

In the correlation map of the DUAL system, we do not observe the negative correlations in areas iii and v that were distinctive to NNI3 (Figure 4C). The absence of these correlations may result from the impact of the VGI ligand in reducing overall enzyme dynamics, a phenomenon noted in our previous studies.[17] We also note reduced intensities of correlations in areas i and ii for the DUAL system compared to NNI3. These areas in the DUAL system are more similar to the corresponding areas in the NNI2 system where there are also reduced correlations relative to the FREE enzyme. Thus, it is likely that the presence of VGI is the reason some of the characteristic correlation patterns observed in NNI3 are reduced in the DUAL system.

Two-dimensional PMF plots also revealed novel conformations when both allosteric ligands are bound compared to the other three systems (Figure 2C). Specifically, DUAL exhibits conformations with the highest degree of closure among all four systems. Some of these conformations are more closed (e.g., interdomain angle of <63°) than the "hyperclosed" conformations previously identified by our group for this enzyme (interdomain angle of ≈63°).[17] With the 3MS ligand participating in many more interactions within the fingers and thumb domains, the ligand spends a considerable amount of time in a vertical position at the apex of the central cavity of the enzyme in the DUAL system. In this position, 3MS is less effective in physically hindering the fingers and thumb domains from coming closer together than in NNI3. However, it would be more efficient in directly blocking access of the RNA template to the enzyme active site (Figure 6B,C). Furthermore, for both NNI2 and DUAL, where the conformations are more closed overall than for NNI3, we observe a hydrogen bond between ARG109 and ASP444 that is not seen in NNI3. It is interesting to note that both these residues are located at the top of the enzyme: Arg109 within the fingers and Asp444 within the thumb. This hydrogen bond would further strengthen interactions that may be important to allosteric communication between the two domains. Finally, the DUAL system also has a hydrogen bond between His95 (fingers domain) and Asn406 (thumb domain) that is not present in the NNI2 system, providing an additional interaction that stabilizes DUAL in a state that is more closed than that of NNI2. Both of these residues are either part of or adjacent to residues making up the RNA duplex channel and thus may be important in the elongation phase of RNA replication.

The regions of the binding site explored by 3MS in the NNI3 system coincide with protein residues known to bind various moieties of different palm allosteric inhibitors (Figure 3C). The yellow snapshot represents a conformation that is very similar to that observed in the cocrystal structure of NS5B with 3MS (PDB entry 3CO9) and is representative of most of the conformations adopted throughout the NNI3 trajectory. In contrast, the purple snapshot shows 3MS in the DUAL system occupying regions that are known to be part of the NNI4 site (Figure 1) and that typically accommodate different palm allosteric inhibitors such as those that contain the benzofuran moiety. These observations, in concert with those discussed above relating to NNI3, suggest that one can consider the two palm sites to be a single large pocket that can accommodate distinct ligands within various regions of the cavity. Thus, the specific location adopted by a given ligand in this extended binding region may depend on its chemical complementarity to different areas of the pocket.

We observe a linear relationship between interdomain angle and template channel width in DUAL that is less pronounced or absent in the other systems (Figure 2). The correlation between these two metrics is readily observed in the 1% lowest-frequency PCA modes of DUAL (see movies in the Supporting Information). These fluctuations entail a highly concerted twisting movement involving all three domains. During this movement, the palm domain is a focal point through which the twisting motion is transferred into the fingers and thumb domains, facilitating their anticorrelated movements relative to

DOI: 10.1021/acs.biochem.5b00411
Biochemistry 2015, 54, 4131−4141

Table 3. Binding Free Energies of the Ligand-Bound Systems Along with the Enthalpic and Entropic Contributions Corresponding to Each

system	ΔH (kcal/mol)	ΔH standard deviation (kcal/mol)	ΔS (kcal mol^{-1} K^{-1})	$T\Delta S$ (kcal/mol)	ΔG^a (kcal/mol)
NNI3	−19.1	16.2	−0.00677	−2.0	−17.0
NNI2	−23.4	3.9	−0.0150	−4.5	−18.9
DUAL	−47.5	8.3	−0.0211	−6.3	−41.2

$^a\Delta\Delta G_{NNI3+NNI2} = -35.9 \pm 20.1$ kcal/mol.

one another. In addition, the thumb and fingers domains of the DUAL system move along different axes. This is in contrast to what is observed in the FREE enzyme, where both the thumb and fingers domains have fluctuations that are along the same axis. Furthermore, the fluctuations in the DUAL system that allow the fingers and thumb domains to come into the proximity of each other also decrease the template channel width, which may make it much more difficult for the RNA template to access the channel and, subsequently, the active site. Such structural changes may disfavor the elongation phase of RNA replication.

The appearance of novel protein conformations in the DUAL system is an emergent property that results from the simultaneous presence of both inhibitors and suggests a nonadditive impact on the NS5B conformational ensemble. These nonadditive effects are consistent with available biochemical evidence that demonstrates synergistic inhibition of NS5B in the combined presence of palm and thumb allosteric inhibitors.[12,13,22]

Novel Conformations in the DUAL System Are Caused by the Altered Interactions of the NNI3 Ligand. As mentioned above, conformations with the highest degree of closure were observed in the DUAL system (Figure 2). The primary determinant of this observation is the flexibility of 3MS, which allows modifications to the hydrogen bonding network between the protein and ligand in the DUAL system. The orientation of 3MS ranges from horizontal to vertical over the course of the DUAL trajectory. The more vertical orientations correspond to a change in hydrogen bonding that allows 3MS to primarily interact with residues in both fingers and thumb domains, stabilizing the enzyme in an extremely closed conformation. Specifically, the ligand makes direct hydrogen bonds with His95, Ala97, and Gln446 and water-mediated hydrogen bonds with residues such as Gly283 in DUAL (Figure 6). In contrast, it makes direct hydrogen bonds with residues such as Thr292, Tyr191, and Tyr448 and water-mediated hydrogen bonds with residues such as Gly449 and Ser288 in NNI3. The majority of protein−ligand hydrogen bonds observed in NNI3 correspond to those identified crystallographically. These hydrogen bonds are weakened or abolished (e.g., those with residues Tyr448, Tyr191, and Thr292) in the DUAL system. In DUAL, we observe new and more stable hydrogen bonds involving residues such as Gln446. In fact, the hydrogen bond between Gln446 and the hydroxyl hydrogen of 3MS has the highest occupancy (84%) of all hydrogen bonds involving protein residues in the DUAL system. This interaction is even more stable than that of Tyr448 (occupancy of 64%), which has the most stable protein−ligand hydrogen bond in NNI3.

3MS adopts numerous conformations and is very mobile in DUAL compared to the NNI3 system (Figure 3C,D). Our studies indicate that these properties are vital to the novel structure and dynamics observed in DUAL. The ability of 3MS to adopt diverse conformations in the DUAL system coincides with the ligand occupying regions of the enzyme that differ from the binding location observed in its original crystal structure (PDB entry 3CO9). For example, in DUAL, 3MS is able to interact with protein residues such as Gln446 and Ile447 with which it did not in NNI3 (Figure 3D). These protein residues have not previously been shown to associate with 3MS. However, they have been shown to interact with other palm allosteric inhibitors with chemical moieties such as benzamide and proline sulfonamide (PDB entries 3LKH and 2GC8). In addition, the conformations that 3MS adopts in DUAL while interacting with these protein residues (Figure 3D) are very different from those observed in NNI3 or for other previously crystallized palm inhibitors. There are instances when 3MS adopts a vertical orientation in the DUAL simulations that allows it to occupy the RNA template channel (Figure 6C and pink-colored ligand in Figure 3D). Thus, when dual inhibitors are bound, NNI3 inhibitors may be particularly effective in preventing the RNA template from accessing the active site. In addition, the high flexibility and mobility of 3MS observed in the DUAL system shed light on the possible difficulty in crystallizing two inhibitors bound to the enzyme, particularly those employed in this work. This may help explain the absence of a NS5B crystal structures containing these two types of inhibitors bound simultaneously.

Nonetheless, our results clearly indicate that the presence of both inhibitors impacts the interactions each ligand makes with the protein and that there are differences in protein−ligand interactions in the singly bound systems versus DUAL. Above, we discussed differences in the hydrogen bonds 3MS makes with the protein in NNI3 versus DUAL. Specifically, in very closed protein conformations, 3MS is able to stabilize interactions between the thumb and fingers domains in the DUAL system, potentially facilitating allosteric communications that can result in inhibition. We also observe changes to the hydrogen bond network of VGI in NNI2 compared to DUAL. We identified water-mediated hydrogen bonds between VGI and Tyr477 and Leu497 in DUAL that were not observed in the NNI2 system. Both of these residues are part of the VGI-binding site. Furthermore, the interaction between VGI and Tyr477 was determined to be crucial for ligand potency.[20] Thus, we can conclude that when both VGI and 3MS are present they facilitate stronger interactions that can disrupt allosteric communication and result in enhanced ligand binding. This observation is further supported by the computed ligand binding energies that are discussed in the next section.

Binding of Dual Ligands Is Energetically Favorable. It is useful to employ the simulation results to understand how the action of these inhibitors relates to their binding efficacies. If enhanced binding occurs in the presence of dual inhibitors, one might expect to observe a relative free energy of binding for the DUAL system that is more favorable than the sum of individual binding free energies for the NNI2 and NNI3 systems. Our calculations indicate that DUAL displays the most favorable computed binding free energy, NNI3 the least

DOI: 10.1021/acs.biochem.5b00411
Biochemistry 2015, 54, 4131−4141

favorable, and NNI2 a value between these two extremes (Table 3). The relative binding free energy computed for the DUAL system ($\Delta\Delta G_{DUAL}$) is more favorable than the sum of binding free energies for the individual systems, $\Delta\Delta G_{NNI3+NNI2}$ (see the last line of Table 3), consistent with synergistic binding of both inhibitors. However, given the uncertainty in the computed values, it is also possible that the inhibitors bind in an additive rather than synergistic manner.

However, the novel patterns of correlation and unique enzyme conformations that arise only when both ligands are present in the DUAL system (Figure 2) clearly indicate that the two ligands jointly impact the enzyme free energy landscape and dynamics. One might anticipate that this observation is associated with synergistic binding of these ligands. Moreover, experimental studies have shown enhanced inhibition when palm and thumb allosteric inhibitors are employed in combination (NNI4 and NNI2 or NNI3 and NNI1),[12,13,22] a situation that also suggests synergistic binding. Thus, despite the estimated uncertainties for the computed free energy values (Table 3), it is likely that both ligands do bind in a slightly synergistic manner.

Regardless of whether these ligands bind in an additive or synergistic manner, our studies indicate that the presence of dual inhibitors does not lower their binding efficacy. Consequently, it is reasonable to anticipate that the net inhibition will be enhanced in the presence of both ligands as suggested by the experimental evidence. Our studies can thus illuminate the molecular mechanisms underlying these observations. We note that the computed affinity of both inhibitors in the DUAL system is more favorable than the affinity of either of the individual NNIs (which are both known to bind to the enzyme). This suggests that both inhibitors should be able to simultaneously bind to the enzyme quite well. It could even be possible that binding occurs in an additive manner, but that once binding takes place the free energy landscape is synergistically modified so that the dual inhibitors are more effective in modulating the physical properties of the enzyme than either on its own.

Broader Significance. We find that the inhibitors studied in this work induce an allosteric response by modulating the ensemble of protein conformations. Recent work shows a link between local interactions and global conformational changes important to allostery.[33,34] Similarly, our work reveals that local differences such as altered hydrogen bonding patterns are associated with distinct global protein properties. Numerous studies have discussed the capacity of allosteric proteins to respond to a ligand in either an agonistic or antagonistic manner based on the presence of a secondary allosteric effector.[35−37] The work presented here provides molecular evidence describing how an allosteric protein such as NS5B can differentially respond to two allosteric inhibitors bound at nonoverlapping sites. Specifically, our results suggest a model of enhanced allosteric inhibition for the HCV polymerase that may include additive binding but also incorporates synergistic changes to protein conformations and fluctuations once both ligands are bound.

As mentioned in the introductory paragraph, one way to combat the viral resistance that arises due to mutations in NS5B is to employ multiple polymerase inhibitors in combination to treat HCV infection. Because allosteric inhibitors do not compete with nucleotides for binding to NS5B, they may be able to reduce the need for widely used nucleoside analogues (such as ribavirin and Solvaldi) that can be associated with nonspecific cellular toxicities. Importantly, our studies suggest that the molecular mechanisms mediating enhanced inhibition for allosteric inhibitors such as those studied in this work may include nonadditive structural and dynamic changes to NS5B.

CONCLUSIONS

We have shown that allosteric inhibitors binding to nonoverlapping locations, specifically sites NNI2 and NNI3, can jointly modulate the conformations and dynamics of the HCV NS5B polymerase. This is true despite the fact that each ligand on its own induces distinct regions of the free energy landscape to be sampled and elicits unique patterns of enzyme motions. We find that the NNI2 inhibitor used in this study elicits its allosteric effect via a conformational selection mechanism in which it stabilizes more closed protein conformations and reduces flexibility compared to the free enzyme. In comparison, the NNI3 ligand not only shifts the population of the enzyme conformation sampled in the free enzyme to be more open on average but also induces novel conformations and correlated motions. The mechanism of action for the NNI3 ligand thus incorporates both conformational selection and induced fit properties. Despite these individual differences, when both NNIs are bound, we observe new protein conformations as well as novel dynamics that were not previously observed in either the free enzyme or the individual enzyme−inhibitor complexes. Although computed binding free energies do not exclude the possibility that the inhibitors bind in an additive manner, they do appear to act synergistically with regard to their ability to modulate enzyme conformations and dynamics. One might anticipate that even if simultaneous binding of both ligands is not more highly favored than the sum of their individual affinities, once both are bound the enzyme may nonetheless undergo dynamics and conformational fluctuations that are more effective in reducing its activity.

These studies provide the first molecularly detailed description of the mechanisms underlying enhanced inhibition of the HCV polymerase in the presence of dual allosteric inhibitors. This knowledge will facilitate efforts to optimize combinations of inhibitors targeting NS5B. In this way, it may be possible to circumvent the emergence of viral resistance that is a persistent obstacle to the development of HCV therapeutics.

ASSOCIATED CONTENT

Supporting Information

Movies describing vibrational modes obtained via principal component analysis of the MD trajectories. The Supporting Information is available free of charge on the ACS Publications website at DOI: 10.1021/acs.biochem.5b00411.

AUTHOR INFORMATION

Corresponding Author

*E-mail: ithorpe@umbc.edu. Telephone: (410) 455-5728. Fax: (410) 455-2608.

Funding

The high performance computing facility (HPCF) at the University of Maryland Baltimore County (UMBC) is funded by the U.S. National Science Foundation through the MRI program (Grants CNS-0821258 and CNS-1228778) and the SCREMS program (Grant DMS-0821311), with significant support from the university. XSEDE is supported by the

DOI: 10.1021/acs.biochem.5b00411
Biochemistry 2015, 54, 4131−4141

National Science Foundation (Grant OCI-1053575). J.A.B. was funded by National Institutes of Health F31 Predoctoral Fellowship GM106958.

Notes

The authors declare no competing financial interest.

■ ACKNOWLEDGMENTS

We employed the UMBC HPCF in this study. This investigation also used the Ranger and Stampede HPC clusters of Extreme Science and Engineering Discovery Environment (XSEDE). We thank Dr. Alexander Sodt for his technical assistance with data analysis. In addition, we acknowledge technical assistance from Meagan Small, Dr. Kenno Vanommeslaeghe, and other members of the laboratory of Dr. Alexander MacKerell. Finally, we thank Ester Sesmero and Brittny Davis and other members of the Thorpe laboratory for numerous and valuable discussions.

■ REFERENCES

(1) Beaulieu, P. L. (2009) Recent advances in the development of NS5B polymerase inhibitors for the treatment of hepatitis C virus infection. *Expert Opin. Ther. Pat. 19*, 145−164.

(2) Leonard B. Seff, J. H. H. (2003) National Institutes of Health Consensus Development Conference: Management of Hepatitis C: 2002. *Hepatology 36*, s1−s2.

(3) Mann, M. P., McHutchison, J. G., Gordon, S. C., Rustgi, V. K., Shiffman, M., Reindollar, R., Goodman, Z. D., Koury, K., Ling, M., and Albrecht, J. K. (2001) Peginterferon α-2b plus ribavirin compared with interferon α-2b plus ribavirin for initial treatment of chronic hepatitis C: A randomised trial. *Lancet 358*, 958−965.

(4) Koch, U. (2006) Allosteric Inhibition of the Hepatitis C Virus NS5B RNA Dependent RNA Polymerase. *Infect. Disord.: Drug Targets 6*, 31−41.

(5) Lindenbach, B. D., and Rice, C. M. (2005) Unravelling hepatitis C virus replication from genome to function. *Nature 436*, 933−938.

(6) Lesburg, C. A. (1999) Crystal structure of the RNA-dependent RNA polymerase from hepatitis C virus reveals a fully encircled active site. *Nat. Struct. Biol. 6*, 937−943.

(7) Bressanelli, S. (1999) Crystal structure of the RNA-dependent RNA polymerase of hepatitis C virus. *Proc. Natl. Acad. Sci. U.S.A. 96*, 13034−13039.

(8) Li, H. (2009) Discovery of (R)-6-Cyclopentyl-6-(2-(2,6-diethylpyridin-4-yl)ethyl)-3-((5,7-dimethyl- [1,2,4]triazolo[1,5-a]-pyrimidin-2-yl)methyl)-4- hydroxy-5,6-dihydropyran-2-one (PF-00868554) as a Potent and Orally Available Hepatitis C Virus Polymerase Inhibitor. *J. Med. Chem. 52*, 1255−1258.

(9) Burton, J. R., Jr., and Everson, G. T. (2009) HCV NS5B polymerase inhibitors. *Clinical Liver Disease 13*, 453−465.

(10) Beaulieu, P. L. (2007) Non-nucleoside inhibitors of the HCV NS5B polymerase: Progress in the discovery and development of novel agents for the treatment of HCV infections. *Curr. Opin. Invest. Drugs 8*, 614−634.

(11) Condon, S. M. (2005) Allosteric Inhibitors of Hepatitis C NS5B RNA-dependent RNA Polymerase. *Curr. Med. Chem.: Anti-Infect. Agents 4*, 99−110.

(12) Le Pogam, S. (2006) Selection and Characterization of Replicon Variants Dually Resistant to Thumb- and Palm-Binding Nonnucleoside Polymerase Inhibitors of the Hepatitis C Virus. *J. Virol. 80*, 6146−6154.

(13) Cheng, C. C., Huang, X., Shipps, G. W., Jr., Wang, Y.-S., Wyss, D. F., Soucy, K. A., Jiang, C.-k., Agrawal, S., Ferrari, E., He, Z., and Huang, H.-C. (2010) Pyridine Carboxamides: Potent Palm Site Inhibitors of HCV NS5B Polymerase. *ACS Med. Chem. Lett. 1*, 466−471.

(14) Adachi, T., Ago, H., Habuka, N., Okuda, K., Komatsu, M., Ikeda, S., and Yatsunami, K. (2002) The essential role of C-terminal residues in regulating the activity of hepatitis C virus RNA-dependent RNA polymerase. *Biochim. Biophys. Acta 160*, 38−48.

(15) Davis, B. C., and Thorpe, I. F. (2013) Molecular Simulations Illuminate the Role of Regulatory Components of the RNA Polymerase from the Hepatitis C Virus in Influencing Protein Structure and Dynamics. *Biochemistry 52*, 4541−4552.

(16) Harrus, D., Ahmed-El-Sayed, N., Simister, P. C., Miller, S., Triconnet, M., Hagedorn, C. H., Mahlas, K., Rey, F., Astier-Gin, T., and Bressanelli, S. (2010) Further Insights into the Roles of GTP and the C Terminus of the Hepatitis C Virus Polymerase in the Initiation of the RNA Synthesis. *J. Biol. Chem. 285*, 32906−32918.

(17) Davis, B. C., and Thorpe, I. F. (2013) Thumb inhibitor binding eliminates functionally important dynamics in the hepatitis C virus RNA polymerase. *Proteins: Struct., Funct., Bioinf. 2013*, 40−52.

(18) Benzaghou, L., Bougie, I., and Bisaillon, M. (2004) Effect of Metal Ion Binding on the Structural Stability of the Hepatitis C Virus RNA Polymerase. *J. Biol. Chem. 279*, 49755−49761.

(19) Bougie, I., Charpentier, S., and Bisaillon, M. (2003) Characterization of the Metal Ion Binding Properties of the Hepatitis C Virus RNA Polymerase. *J. Biol. Chem. 278*, 3868−3875.

(20) Ontoria, J. M. (2009) Identification and Biological Evaluation of a Series of 1H-Benzo[de]isoquinoline-1,3(2H)-diones as Hepatitis C Virus NS5B Polymerase Inhibitors. *J. Med. Chem. 52*, 5217−5227.

(21) Ruebsam, F. (2008) Pyrrolo[1,2-b]pyridazin-2-ones as potent inhibitors of HCV NS5B polymerase. *Bioorg. Med. Chem. Lett. 18*, 3616−3621.

(22) Liu, Y., Donner, P. L., Pratt, J. K., Jiang, W. W., Ng, T., Gracias, V., Baumeister, S., Wiedeman, P. E., Traphagen, L., Warrior, U., Maring, C., Kati, W. M., Djuric, S. W., and Molla, A. (2008) Identification of halosalicylamide derivatives as a novel class of allosteric inhibitors of HCV NS5B polymerase. *Bioorg. Med. Chem. Lett. 18*, 3173−3177.

(23) MacKerrel, A. D., Brooks, B., Brooks, C. L., III, Nilsson, L., Roux, B., Won, Y., and Karplus, M. (1998) CHARMM: The Energy Function and its Parameterization. In *Encyclopedia of Computational Chemistry*, John Wiley and Sons, Ltd., New York.

(24) Vanommeslaeghe, K., Hatcher, E., Acharya, C., Kundu, S., Zhong, S., Shim, J., Darian, E., Guvench, O., Lopes, P., Vorobyov, I., and MacKerell, A. D., Jr. (2010) CHARMM General Force Field: A Force Field for Drug-Like Molecules Compatible with the CHARMM All-atom Additive Biological Force Fields. *J. Comput. Chem. 31*, 671−690.

(25) MacKerell, A. D., Jr., Bashford, D., Bellot, M., Dunbrack, R. L., Evanseck, J. D., Field, M. J., Fischer, S., Gao, J., Guo, H., Ha, S., Joseph-McCarthy, D., Kuchnir, L., Kuczera, K., Lau, F. T. K., Mattos, C., Michnick, S., Ngo, T., Nguyen, D. T., Prodhom, B., Reiher, W. E., III, Roux, B., Schlenkrich, M., Smith, J. C., Stole, R., Straub, J., Watanabe, M., Wiorkiewicz-Kuczera, J., Yin, D., and Karplus, M. (1998) All-Atom Empirical Potential for Molecular Modeling and Dynamics Studies of Proteins. *J. Phys. Chem. B 102*, 3586−3616.

(26) Biswal, B. K., Cherney, M. M., Wang, M., Chan, L., Yannapoulos, C. G., Bilimoria, D., Nicolas, O., Bedard, J., and James, M. N. G. (2005) Crystal Structures of the RNA-dependent RNA Polymerase Genotype 2a of Hepatitis C Virus Reveal Two Conformations and Suggest Mechanisms of Inhibition by Non-nucleosdie Inhibitors. *J. Biol. Chem. 280*, 18202−18210.

(27) Chinnaswamy, S., Murali, A., Yi, G., Palaninathan, S., and Kao, C. C. (2010) Conformations of the monomeric hepatitis C virus RNA-dependent RNA polymerase. *Virus Adapt. Treat. 2*, 21−39.

(28) Lee, M. S., Feig, M., Salsbury, F. R., Jr., and Charles, C. L., III (2003) New analytic approximation to the standard molecular volume definition and its application to generalized Born calculations. *J. Comput. Chem. 24*, 1348−1356.

(29) Feig, M., Onufriev, A., Lee, M. S., Im, W., Case, D. A., and Brooks, C. L., III (2004) Performance comparison of generalized Born and Poisson methods in the calculation of electrostatic salvation energies for protein structures. *J. Comput. Chem. 25*, 265−284.

(30) Chocholousova, J., and Feig, M. (2006) Balancing an accurate representation of the molecular surface in generalized Born formalisms

DOI: 10.1021/acs.biochem.5b00411
Biochemistry 2015, 54, 4131−4141

with integrator stability in molecular dynamics simulations. *J. Comput. Chem. 27*, 719−729.
(31) Tzoupis, H., Leonis, G., Mavromoustakos, T., and Papadopoulos, M. G. (2013) A Comparative Molecular Dynamics, MM-PBSA and Thermodynamic Integration Study of Saquinavir Complexes with Wild-Type HIV-1 PR and L10I, G48V, L63P, A71V, G73S, V82A and I84V Single Mutants. *J. Chem. Theory Comput. 9*, 1754−1764.
(32) Moustafa, I. M., Shen, H., Morton, B., Colina, C. M., and Cameron, C. E. (2011) Molecular Dynamics Simulations of Viral RNA Polymerases Link Conserved and Correlated Motions of Functional Elements to Fidelity. *J. Mol. Biol. 410*, 159−181.
(33) Motlagh, H. N., and Hilser, V. J. (2012) Agonism/antagonism switching in allosteric ensembles. *Proc. Natl. Acad. Sci. U.S.A. 109*, 4134−4139.
(34) Cui, Q., and Karplus, M. (2008) Allostery and cooperativity revisited. *Protein Sci. 17*, 1295−1307.
(35) Hol, T., Cox, M. B., Bryant, H. U., and Draper, M. W. (1997) Selective estrogen receptor modulators and postmenopausal women's health. *Journal of Women's Health 6*, 523−531.
(36) Katzenellenbogen, B. S., Montano, M. M., Ekena, K., Herman, M. E., and McInerney, M. E. (1997) Antiestrogens: Mechanisms of action and resistance in breast cancer. *Breast Cancer Res. Treat. 44*, 23−38.
(37) Lu, N. Z., and Cidlowski, J. A. (2005) Translational regulatory mechanisms generate N-terminal glucocorticoid receptor isoforms with unique transcriptional target genes. *Mol. Cell 18*, 331−342.

DOI: 10.1021/acs.biochem.5b00411
Biochemistry 2015, 54, 4131−4141